Available online at www.sciencedirect.com
ScienceDirect
Journal of Sound and Vibration 324 (2009) 1158–1180
JOURNAL OF SOUND AND VIBRATION
www.elsevier.com/locate/jsvi

A new damage detection approach for beam-type structures based on the combination of continuous and discrete wavelet transforms

Hakan Gökdağ*, Osman Kopmaz

Uludağ University, Faculty of Engineering and Architecture, Mechanical Engineering Department, 16059 Görükle-Bursa, Turkey

Received 2 July 2008; received in revised form 23 February 2009; accepted 24 February 2009
Handling Editor: C.L. Morfey
Available online 5 April 2009

Abstract

In this work, a new wavelet-based damage detection approach has been proposed. The method is based on the assumption that a damaged mode shape of a beam is approximately composed of an undamaged mode and other contributors such as measurement- and local damage-induced variations. Then, a proper approximation function (AF) to be used as undamaged mode can be extracted from the damaged one by the discrete wavelet transform (DWT), provided a suitable wavelet and a decomposition level (DL) are determined. By this way, a reliable damage index can be defined taking the difference of the continuous wavelet transform (CWT) coefficients of the damaged mode and those of the AF. It is demonstrated that the AF which is well-correlated with the numerical undamaged mode of beam can be obtained at the DL after which the approximation energy ratio (Ea) drops significantly, if a suitable wavelet having sufficient number of vanishing moments (NVM) is selected. In order to test the method, the first two numerically obtained modes of a damaged beam as well as the first two experimental modes of another damaged beam are employed. Although the physical properties and damage features of these two beams are quite different, it is concluded that the AFs which are derived from these modes by the proposed method can be conveniently used as baseline data for damage detection purpose.

1. Introduction

Recently, wavelet analysis has become a widely used signal processing tool in the field of vibration-based damage detection due to its promising features such as singularity detection, good handling of noisy data, being very informative about damage location/time and extent. For this reason, many studies on damage detection are based on the wavelet transform scheme. An extensive literature survey on the subject is available in the work of Kim and Melhem [1], with specific applications including beam crack detection and gear, or roller damage detection.

In this study, the main subject is damage detection through processing spatial data (especially mode shapes) by the wavelet transform. The works recently published in this context can be classified into two groups

*Corresponding author. Tel.: +90 224 294 19 98.
E-mail address: hakangkd@uludag.edu.tr (H. Gökdağ).

0022-460X/$ - see front matter © 2009 Elsevier Ltd. All rights reserved.
doi:10.1016/j.jsv.2009.02.030

according to the dependence on healthy data, i.e., the researches in the first group only employ the spatial data of defected structure, whereas those in the other group need the knowledge of intact structure as well as the damaged one.

Some representative examples of the first group are Refs. [2–13]. In these works, while the damaged structure is frequently a beam, other elements such as plane frames [7], plates as a bidimensional structure [9,12] are also considered. Although the signal to be processed by the wavelet transform is often mode shape of damaged structure, other spatial data such as static/dynamic displacement profiles of a cracked beam carrying a discrete load, and displacement response of a plate subjected to in-plane stress are also employed [2]. The damage detection procedure is carried out in three steps: First, the spatial data are obtained through one of the methods: analytical solution, finite element method, and experiment. Second, it is transformed into the scale-shift domain by the wavelet transformation. In this stage, it is the continuous wavelet transform (CWT) that is mostly preferred as a tool, because it provides redundant information, which enhances damage identification. On the other hand, the discrete wavelet transform (DWT), which enables faster computation, is also reported to work in some cases [7]. Moreover, Zhong and Oyadiji [13] have recently developed a stationary wavelet transform (SWT)-based approach for the beams with symmetric end conditions. Although their method requires that the beam ends be symmetric, which is the main restriction of the method, the authors demonstrated that it outperforms other classic SWT- and DWT-based approaches. At the third step, wavelet coefficient function at each scale is examined in the case of the CWT to seek damage signatures arising in the form of sudden sharp peaks for the lower scales. Likewise, the detail coefficients have damage information in the case of the DWT. On the other hand, experimental noise is inevitable for real data, hence its influence on wavelet coefficients are investigated in some works by means of the Hoelder and Lipschitz exponents [3,4]. From these studies it is concluded that the lower scales should be ignored during damage detection, since they are affected the most by noise. Moreover, wavelet modulus of noise was observed to have a negative Hoelder exponent, which means the modulus decreases as the scale rises in contrast to the wavelet modulus due to damage. It is therefore possible to distinguish between noise- and damage-induced peaks. Another significant issue dealt with in several of the above studies is the choice of the analyzing wavelet. In this context, emphasis is placed on some concepts such as the number of vanishing moments (NVM), the regularity, and the symmetry of wavelets.

As to the second group, the entire procedure in these papers is similar to those of the first group to a great extent except that the healthy data are also wavelet transformed. Thus, wavelet coefficients of the healthy signal are generally subtracted from the damaged coefficients [14,15]. In this way, one can perform damage identification by examining the difference of transform coefficients. In another work [16], the damage index defined as $\alpha = \log_2|Wf(u_d,s)|/\log_2|Wf_0(u_d,s)|$ is employed to determine crack location and extent, where $Wf(u_d,s)$ and $Wf_0(u_d,s)$ refer to damaged and undamaged transform coefficients, respectively. In that work, the analyzed signal is the time dependent displacement measured from a point on the beam during the course of the load moves across the beam length. However, the procedure is similar to that of the above works where the CWT is considered.

The significant drawback of the methods in the second group is that healthy data may not exist for many structures, especially for the old ones. Therefore, much effort has been made to develop methods requiring only damaged data. However, an important issue with these methods is the border distortion problem. As real signals are of finite length, there occur high-valued transform coefficients at the ends of signal, which may lead to misleading results about damage detection. To overcome this deficiency, several solutions such as windowing [5], extending signal through extrapolation [12], etc., are suggested. Nevertheless, as stated in Ref. [13], the methods employing only damaged data have turned out to be insufficient to identify crack-like damages when sampling distance enlarges as well as crack size decreases. Hence, employing healthy data in such cases can be considered as a remedy for the problem. Moreover, the border distortion problem is eliminated via extracting healthy wavelet coefficients from damaged counterparts.

In view of the above consideration, a new method employing only damaged structure data but holding the advantages of the methods that also use healthy structure data is demanded. Therefore, a different approach deriving an approximately equivalent of undamaged mode from damaged one is introduced in this paper, considering beam-type structures. To this end, the following steps are applied: First, mode shape is extended at the ends to reduce border distortion. Later, a proper approximation function (AF) is extracted from this

extended signal through the DWT in order to utilize it as baseline data. In this stage, it is explained which wavelet and decomposition level (DL) are suitable in order to obtain the proper AF. For that purpose, the relation among NVM, DL, the modal assurance criterion (MAC), and Ea are illustrated by graphs. Finally, both the damaged mode and the extracted AF are continuous wavelet transformed, and their difference is employed as damage index. The accuracy of the method is validated using the first two numerically obtained modes of a damaged beam as well as the first two experimental modes of another damaged beam. Although the physical properties and damage conditions of these two beams are quite different, the proposed method revealed sufficiently accurate results for both of them.

2. Theory

2.1. The main features of the CWT and the DWT

The wavelet transform of a continuous signal, $x(t)$, can be defined as

$$T(a,b) = a^{-1/2}\int_{-\infty}^{\infty} x(t)\psi^*_{a,b}(t)\,\mathrm{d}t \tag{1}$$

where $\psi_{a,b}(t)$ is obtained from the mother wavelet $\psi(t)$ which satisfies some mathematical requirements as $\psi_{a,b}(t) = \psi((t-b)/a)$ by the scale (a) and dilation (b) parameters (both are real and $a \neq 0$), overstar denotes complex conjugate (a wavelet may in general be complex) [17]. In mathematical terms, Eq. (1) is called convolution, and shows how well a wavelet function correlates with the signal $x(t)$. Sharp transitions in $x(t)$ yield wavelet coefficients of large amplitudes [7], which is the premise of the CWT-based damage detection. To capture damage-induced changes, suitable wavelets must be chosen. The suitability of a wavelet is, to a great extent, related to its NVM. If the wavelet $\psi(t)$ is defined as $\psi(t) := \mathrm{d}^M\phi(t)/\mathrm{d}t^M$, where $\phi(t)$ denotes a piecewise smooth function of M-times differentiable and satisfying some other technical restrictions, then it is said to have M vanishing moments, if it is orthogonal to the polynomials up to degree $M-1$, i.e. $\int_{-\infty}^{\infty}\psi(t)t^m\,\mathrm{d}t = 0$, $(m = 0,1,\ldots,M-1)$ [17,18]. Hong et al. [3] suggest that wavelets should have at least two vanishing moments to detect crack employing beam modes. Besides, Douka et al. [4] state that wavelets with higher NVM provide more stable performance when damaged beam modes are considered. However, localization of wavelets deteriorates with rising NVM, thus the tradeoff between localization and stable performance should be considered.

The CWT is known to be redundant transformation. However, this redundancy can be removed by the special arrangement of the scale and the dilation parameters called "dyadic sampling". In this case Eq. (1) takes the form

$$T_{m,n} = \int_{-\infty}^{\infty} x(t)2^{-m/2}\psi_{m,n}(t)\,\mathrm{d}t \tag{2}$$

where $\psi_{m,n}(t) = \psi(2^{-m}t - n)$, and the integers m and n are related to the scale and the dilation parameters, respectively. Orthonormal dyadic discrete wavelets are associated with scaling functions and their dilation equations. The scaling function has the same form as the wavelet, given by $\phi_{m,n}(t) = 2^{-m/2}\phi(2^{-m}t - n)$. They have the property $\int_{-\infty}^{\infty}\phi_{0,0}(t) = 1$, where $\phi_{0,0}(t) = \phi(t)$ is sometimes called as father scaling function or father wavelet. If the scaling function is convolved with the original signal, one obtains the *approximation coefficients* at the mth level as $S_{m,n} = \int_{-\infty}^{\infty} x(t)\phi_{m,n}(t)$. Then, continuous approximation of the signal at the mth level, i.e. the AF, can be generated by

$$x_m(t) = \sum_{n=-\infty}^{\infty} S_{m,n}\phi_{m,n}(t) \tag{3}$$

where $x_m(t)$ is a smooth version of the signal $x(t)$. Finally, the original signal $x(t)$ can be represented using both the AF at an arbitrary m_0th level and the sum of signal details from m_0 down to infinity as follows:

$$x(t) = x_{m_0}(t) + \sum_{m=-\infty}^{m_0} d_m(t) \tag{4}$$

where $x_{m_0}(t) = \sum_{n=-\infty}^{\infty} S_{m_0,n}\phi_{m_0,n}(t)$, $d_m(t) = \sum_{n=-\infty}^{\infty} T_{m,n}\psi_{m,n}(t)$. From this equation it can be concluded that $x_{m-1}(t) = x_m(t) + \mathrm{d}_m(t)$. Accordingly, the signal approximation at an increased resolution, i.e. at a smaller scale, can be obtained by adding the signal detail and approximation at the level m. This kind of representation is called multiresolution [17].

2.2. The damage identification scheme

The method is based on the principle assumption that damaged mode ($M_d(x)$) is approximately equal to the sum of local damage-induced variations ($\eta(x)$) and corresponding undamaged mode ($M_u(x)$), i.e. $M_d = M_u + \eta$. Moreover, M_u contains some noise which is due to computational errors if M_u is obtained numerically, or measurement errors if M_u is measured experimentally. Besides, this noise has, in general, both high- and low-frequency parts [13]. Hence, when M_d is decomposed by the DWT, one expects that the AF at a suitable DL contains only lower-frequency part, while high-frequency noise and damage effects appear in detail functions. Here, η is assumed to be available in the DWT details [7]. If the energy of high-frequency part of noise in M_u is relatively lower order, then there will probably be remarkable resemblance between M_u and the extracted AF, since low-frequency components are dominant in both signals. However, one cannot guarantee that the AF is exactly the equivalent of M_u because of noise and the inherent characteristic of the DWT. That is, in the DWT, signal is decomposed to only scales of some powers of 2, so that the frequency content of the AF may not be exactly the same as M_u. Nevertheless, one can extract an AF which is in relatively good agreement with M_u by the proposed procedure.

A restriction of the method is that sudden section variations should not be in the span where modal data are measured. Because, there may be discontinuities in derivatives of data due to these local variations. Therefore, an AF extracted in this case may be free of such discontinuities, so that it may far from resembling to M_u. Now, the four steps of the method are elucidated as follows:

(I) *Mode shape extension*: Before processing M_d by the DWT, it is subjected to some preparations to increase the efficiency of the wavelet transform. In this context, M_d is extended first to reduce border distortion. There are other ways for this as cited above, but here a mode function is extended asymmetrically by itself at the ends, as shown in Fig. 1. The original signal, M_d, is rotated 180° about the origin, and added to its left end. Similarly, it is rotated 180° about the right end, and added to the right end of the original mode. In this way, continuity in function as well as odd derivatives at data ends are achieved [19]. If the length of M_d is n, one obtains a signal of length $(3n–2)$ after the extension.

(II) *Upsampling to the nearest power of* 2: Since the DWT is defined for sequences with the length of some power of 2 [20], the extended signal is upsampled to the nearest power of 2 by the cubic spline interpolation.

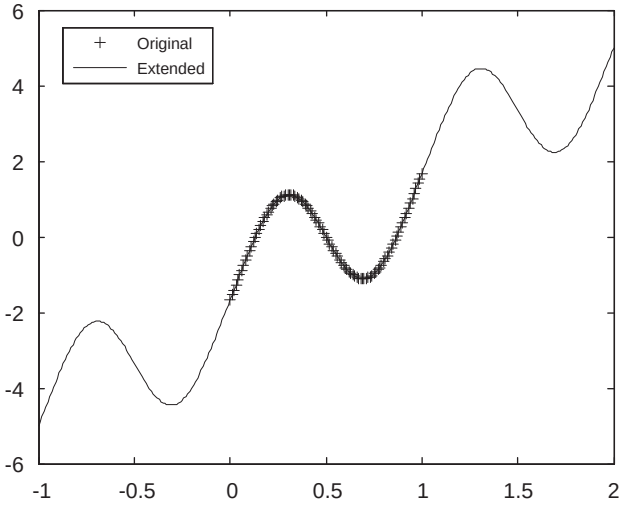

Fig. 1. Extension of a mode shape.

(III) *Extracting the most suitable AF*: This is the most significant stage of the method. Here, after choosing a wavelet, it is decided which NVM and DL are suitable to obtain an AF which is very compatible with M_u. To achieve a complete decomposition of signal, it is significant to select an orthogonal wavelet basis. Then, we have alternatives such as Daubechies, symlet, Coiflet, biorthogonal, and reverse biorthogonal families [20]. In this work, symlet and Daubechies wavelets are regarded, since similar performances were observed for the rest. On the other hand, to demonstrate how much an extracted AF is close to M_u, we used MAC index, one of the widely employed tools in the experimental modal testing, and defined for two mode sequences S_1 and S_2 (these may be complex in general) of length $\overline{N}$ as [21]

$$\mathrm{MAC}(S_1,S_2)=\frac{|\sum_{k=1}^{\overline{N}}S_1(k)S_2^*(k)|^2}{(\sum_{k=1}^{\overline{N}}S_1(k)S_1^*(k))(\sum_{k=1}^{\overline{N}}S_2(k)S_2^*(k))} \tag{5}$$

Moreover, the MACs defined for their first and second derivatives are also considered to ensure that the two, i.e. the AF and the numerically obtained M_u, are in fact well-correlated, because the CWT is known to be sensitive to the variations in derivatives of signal. Then, there are three MACs; one for the functions themselves (MAC1 = MAC(AF, M_u)), another one for their first derivatives (MAC2 = MAC(AF′, M_u')), and the last one between their curvatures (MAC3 = MAC(AF″, M_u'')), where prime denotes derivative with respect to spatial coordinate ($' = \mathrm{d}/\mathrm{d}x$). The MACs of higher-order derivatives are not taken into account, since they have relatively arbitrary variation, which is normal because of high-frequency measurement noise in M_u. In other words, higher-order derivatives are sensitive to the higher-frequency components in data. However, an extracted AF represents the lower-frequency parts of data, thus it is not reasonable to expect the MACs of higher-order derivatives to be as large as the lower-order derivatives. An AF making the three MACs comparatively great is a good candidate to be employed as an undamaged mode. However, it is not practically possible to compute these MACs if healthy data are unavailable. Therefore, another indicator which shows that an extracted AF is suitable is needed. In this context, the approximation energy ratio (Ea), which can be given in discrete form as

$$\mathrm{Ea(percent)}=100\frac{\sum_{k=0}^{N-1}x_{m_0}(k)^2}{\sum_{k=0}^{N-1}x(k)^2}\quad N:\ \text{signal length} \tag{6}$$

according to Eq. (4), is proposed. It was observed that the three MACs have relatively great values at the DL after which there occurs the first notable decrease in Ea. This happens especially for higher NVMs.

The relation among the suitable AF, large NVMs, and sudden drop in Ea can be explained as follows: As NVM rises; frequency spectrums of wavelet and associated scale function become more flat about zero frequency, and their localizations increase [17,22]. Practically, this means that an AF obtained by a wavelet with larger NVM has lower-frequency content, thus it can be expected to be closer to M_u, provided high-frequency measurement errors in M_u are sufficiently low. In Fig. 3.15 of Ref. [17], variation of frequency spectrums of Daubechies wavelet and associated scale function versus NVM is given. According to that figure, there seems little shrinkage in spectrums for NVM > 9, thus spectrums for NVM = 10 and 20 are nearly the same. In addition, we experienced the same trend for symlet wavelets, and concluded that NVM > 20 can be ignored. Besides, such large NVMs may cause computational problems. Therefore, it is possible to conclude that the interval between 10 and 20 is adequate for proper NVMs. After choosing a NVM value from this interval, the trend of Ea along with DL is observed to determine the suitable DL. In the DWT, scale (a) and DL are related as $a=2^{\mathrm{DL}}$, i.e. the increase of scale is remarkable for larger DLs. Since scale and frequency are inversely related [17], frequency spectrum of scale function decreases sharply for greater DLs. However, lower-frequency parts are dominant in M_u, and they represent the significant part of the signal energy. Hence, after a critic DL, the AF loses some low-frequency components which are more dominant in M_u than other high-frequency components, then a sudden drop in Ea occurs. In this case, we propose to regard the previous DL, since it is the last value for higher-frequency components to leave the AF. After this threshold, the essential parts of M_u are begun to be eliminated, so that the drop in Ea becomes significant. Although the suitable DL is 2 for the beams considered in this work, this may be greater if modal data are denser.

To summarize, one can extract a suitable AF at the DL after which the first notable drop in Ea occurs, if the symlet wavelet with NVM between 10 and 20 is used.

(IV) *Calculation of damage index*. The wavelet coefficients of the extracted AF and M_d, $T_A(a,b)$ and $T_d(a,b)$, respectively, are computed by the CWT, and the following damage indexes are introduced similar to that in Ref. [15]:

$$D_1 = |T_d(a,b) - T_A(a,b)| \tag{7}$$

$$D_2 = |T_d(a,b) - T_u(a,b)| \tag{8}$$

where $T_u(a,b)$ refers to the wavelet coefficients of M_u obtained numerically. If a suitable AF is extracted from damaged mode, these indexes are expected to be compatible.

3. Experimental procedure

To validate the suggested approach by real data, the first two experimental modes of a free–free beam with multiple notches are measured. The physical properties of the beam are given in Fig. 2(a). Here, apart from the previous works where experimental modes of damaged beam are considered (such as [3,5,10,12]), eight notches are cut on the beam by a handsaw to provide (1) closely spaced damages of different extents, (2) damages close to ends, and (3) different-extent-damages on the same location. For that purpose, two types of notches are considered as shown in Fig. 2(b). The features of all the eight defects are presented in Table 1, where I and VIII satisfy the above second condition, while III–IV and V–VI pairs are for the first condition. In addition, II and VII are for the third condition, since they are symmetrically located on the beam. Impact testing as in Ref. [12] is implemented to extract mode shapes. To this end, 73 equally spaced measurement points are chosen as shown in Fig. 2a. Note that the first and the 73rd points are 3.5 mm away from free ends, because it is difficult to avoid double hits on a point very close to free end. Later, in order to satisfy free end conditions,

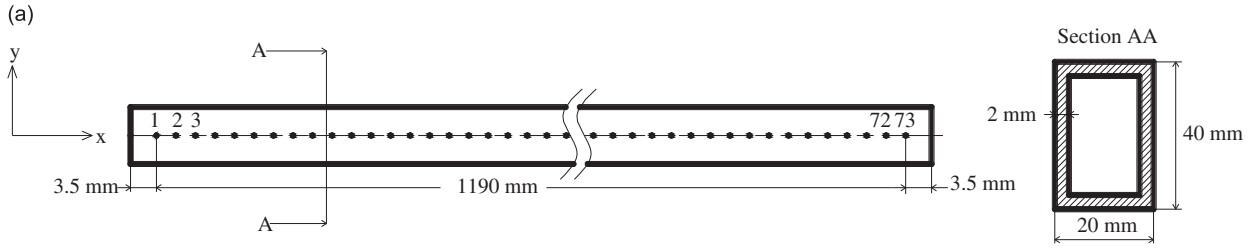

$E = 198$ GPa (Young's modulus), $\rho = 7608$ kgm^{-3} (the measured density), $\nu = 0.3$ (Poisson's ratio).

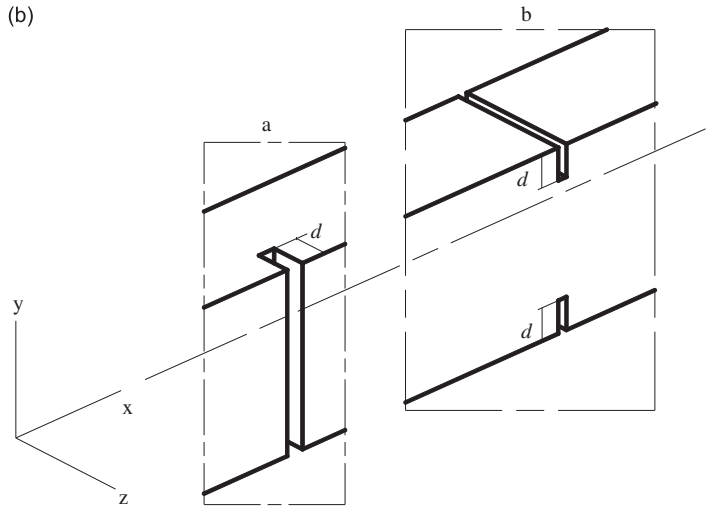

Fig. 2. (a) The physical properties of the beam whose experimental mode shapes were measured. Points numbered from 1 to 73 refer to the measurement locations. (b) Two different notch types on that beam. a: across the long edge, b: across the short edge, and two sided, *d*: depth.

Table 1
Damage features of the beam depicted in Fig. 2.

Damage no. →	I	II	III	IV	V	VI	VII	VIII
Between the measurement points	1–2	13–14	31–32	32–33	40–41	41–42	60–61	71–72
Distance ratio to the point 1	6.94e−3	0.1736	0.4236	0.4375	0.5486	0.5625	0.8264	0.9791
Damage type (see Fig. 2b)	a	a	a	b	a	b	b	a
Notch depth (d) (see Fig. 2b) (mm)	6	4	3	3	3	3	3	3

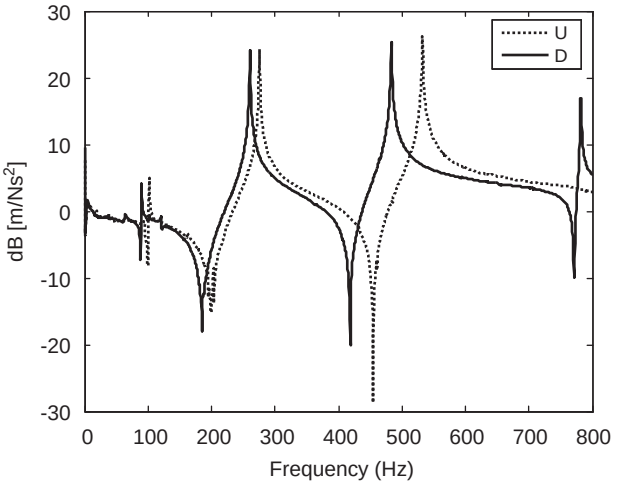

Fig. 3. Experimental FRFs measured from the 19th point for damaged (D) and undamaged (U) cases of the beam in Fig. 2. The first three undamaged beam natural frequencies (Hz) are 101.5, 275.5, 532.0 (experimental), and 101.43, 276.96, 541.72 (ANSYS). Experimental natural frequencies (Hz) of the damaged beam are 89, 260.5, 483.5.

the beam is hung on the points which correspond to the nodes of the first undamaged mode (one in the middle of points 17 and 18, and the other one between 56 and 57) through fish lines of the same length. An accelerometer (Brüel&Kjaer Type 4514) is mounted at the 19th point, and six impacts are applied by a modal hammer (Brüel&Kjaer Type 8206-003) at each one of the 73 points along the $-z$ direction, so that experimental noise is tried to average out. Then, these signals are sent to a laptop through an ADC (Brüel&Kjaer PC Card Front End 3560-L) to compute the frequency response functions (FRFs). In Fig. 3 the FRFs measured from the 19th point, i.e. the driving point, both for damaged and undamaged cases are illustrated. To check the reliability of the experiments, the first two undamaged beam natural frequencies are measured, and compared to those from the finite element model solved by ANSYS. The reason of using ANSYS instead of exact solution is that the influence of the accelerometer mass over FRFs is observed to be significant; therefore its mass is accounted for by modeling as an additional discrete mass. The agreement between the results is obvious as seen in the legend of Fig. 3; hence, one can conclude that the damaged beam modes are obtained sufficiently accurate, since the same experimental procedure is implemented both for the damaged and undamaged cases of the beam. For such a lightly damped beam, the peak picking method [21] can be utilized to obtain the first several mode shapes. The first and second damaged modes extracted in this way are illustrated in Fig. 4 (the third mode was observed to be comparatively erroneous, hence it is discarded). In this figure the numerically obtained modes of the undamaged beam are also shown for comparison.

4. Simulation results

As stated above, the most significant stage of the proposed method is the third step, where a suitable AF is extracted in order to employ instead of M_u. According to the method, at the DL after which Ea drops

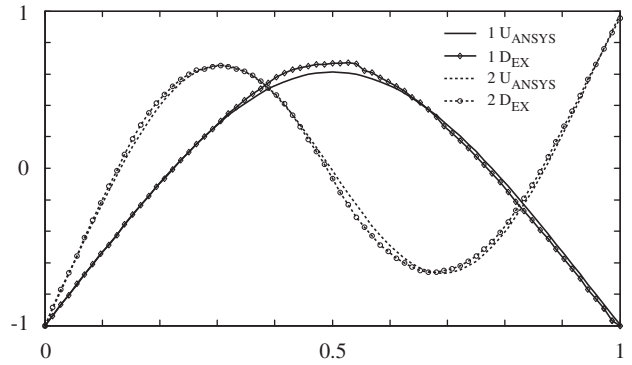

Fig. 4. The first two experimental damaged (D_{Ex}) and numerically obtained undamaged (U_{ANSYS}) modes of the free–free beam in Fig. 2. Horizontal axis denotes the normalized beam length (x/L), while the vertical one stands for the normalized amplitude.

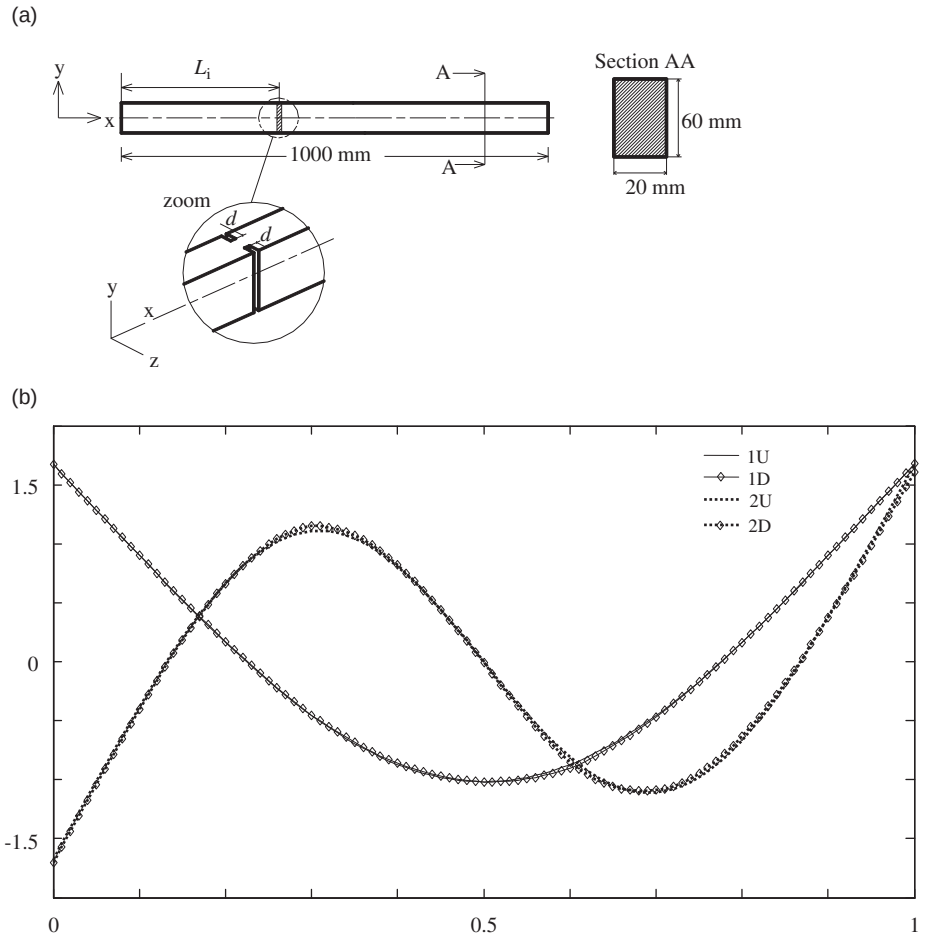

Fig. 5. (a) The second beam containing four notches; $L_1 = 5$ mm, $L_2 = 300$ mm, $L_3 = 600$ mm, $L_4 = 610$ mm. $d = 5$ mm for all notches. Material properties: $E = 3.42$ GPa (Young's modulus), $\rho = 1187\,\mathrm{kg\,m^{-3}}$ (density), $\nu = 0.32$ (Poisson's ratio). Natural frequencies (Hz) of the damaged beam obtained by ANSYS: 34.87, 96.02. (b) The first two damaged (D) and undamaged (U) modes of this beam obtained by ANSYS. 1: The first mode, 2: The second mode.

significantly, the MAC3 as well as MAC1 and MAC2 have relatively great values for higher NVMs. Hence, at this DL, the suitable AF can be obtained. To verify this assertation, the first two damaged modes of another beam with different physical and defect properties (Fig. 5) are considered in addition to the experimental

modes shown in Fig. 4. Now, there are four mode shapes to be analyzed; the first two modes of the damaged beam shown in Fig. 5, which were obtained numerically by ANSYS, and the first two experimental modes of the damaged beam depicted in Fig. 2. In the following, variations of Ea and MACs wrt NVM and DL are demonstrated employing these four modes to make comprehensive how the proper AF is derived. To compute a MAC, the related undamaged beam mode is needed. Therefore, all undamaged beam modes were obtained by ANSYS in advance.

Table 2
Variations of the MACs and Ea wrt DL and NVM.

DL	MAC1	MAC2	MAC3	Ea	DL	MAC1	MAC2	MAC3	Ea
	Wavelet: sym2					Wavelet: sym3			
1	0.9999	0.9992	0.2351	100.0000	1	0.9999	0.9995	0.8910	100.0000
2	0.9998	0.9847	0.0157	99.9989	2	0.9999	0.9994	0.7253	99.9985
3	0.8999	0.3899	0.0003	98.3853	3	0.9752	0.8379	0.0108	99.5099
4	0.0003	0.0453	0.0003	85.9138	4	0.0004	0.0091	0.0042	83.8460
	Wavelet: sym4					Wavelet: sym5			
1	0.9999	0.9995	0.9114	100.0000	1	0.9999	0.9995	0.9176	100.0000
2	0.9999	0.9995	0.9239	99.9980	2	0.9999	0.9995	0.9477	99.9975
3	0.9928	0.9620	0.1712	99.6712	3	0.9971	0.9874	0.6454	99.7914
4	0.0004	0.0023	0.0128	91.5956	4	0.0004	0.0204	0.5374	93.9781
	Wavelet: sym6					Wavelet: sym7			
1	0.9999	0.9995	0.9191	100.0000	1	0.9999	0.9995	0.9173	100.0000
2	0.9999	0.9995	0.9669	99.9931	2	0.9999	0.9995	0.9624	99.9939
3	0.9988	0.9958	0.8873	99.8144	3	0.9981	0.9954	0.9528	99.7596
4	0.0004	0.0097	0.2302	94.2498	4	0.0003	0.1704	0.7086	93.8258
	Wavelet: sym8					Wavelet: sym9			
1	0.9999	0.9995	0.9211	100.0000	1	0.9999	0.9995	0.9224	100.0000
2	0.9999	0.9995	0.9713	99.9912	2	0.9999	0.9995	0.9725	99.9803
3	0.9990	0.9976	0.9743	99.8297	3	0.9991	0.9977	0.9798	99.8518
4	0.0004	0.0137	0.5371	95.9441	4	0.0004	0.0055	0.7721	96.5646
	Wavelet: sym10					Wavelet: sym11			
1	0.9999	0.9995	0.9218	100.0000	1	0.9999	0.9995	0.9192	100.0000
2	0.9999	0.9995	0.9677	99.9924	2	0.9999	0.9995	0.9737	99.9952
3	0.9987	0.9972	0.9784	99.8152	3	0.9985	0.9957	0.9534	99.8055
4	0.0004	0.1294	0.6844	96.9182	4	0.0004	0.0442	0.6954	96.7390
	Wavelet: sym12					Wavelet: sym13			
1	0.9999	0.9995	0.9216	100.0000	1	0.9999	0.9995	0.9231	100.0000
2	0.9999	0.9995	0.9688	99.9981	2	0.9999	0.9995	0.9698	99.9990
3	0.9985	0.9971	0.9796	99.8438	3	0.9983	0.9955	0.9567	99.7271
4	0.0004	0.8077	0.6869	97.4646	4	0.0004	0.0530	0.6840	97.9360
	Wavelet: sym14					Wavelet: sym15			
1	0.9999	0.9995	0.9218	100.0000	1	0.9999	0.9995	0.9198	100.0000
2	0.9999	0.9995	0.9731	99.9984	2	0.9999	0.9995	0.9676	99.9983
3	0.9986	0.9973	0.9818	99.7991	3	0.9979	0.9941	0.9374	99.7297
4	0.0004	0.4650	0.6892	97.9263	4	0.0004	0.1469	0.6975	97.7331

For symN ($N = 1,2,\ldots$), N denotes NVM. The values were computed using the first numerically obtained damaged mode of the beam in Fig. 5.

4.1. Extracting the most suitable AF

Applying the damage identification scheme to the first numerically obtained damaged mode of the beam in Fig. 5, the values in Table 2 are found at the third step. In view of the Table 2, MAC1 is observed to have relatively large values at the first two DLs for all NVM. At the third level, there occurs slight decrease, and then it drastically drops at the fourth level, which means that the AF at the fourth level is useless regardless of MAC2, MAC3, and NVM. Hence, it is apparent that the first three DLs should be considered. When NVM is greater than 3, similar variation is available for MAC2 with rising level. On the other hand, MAC3 have smaller amounts at all DLs for lower NVMs, while for upper NVMs its values are relatively high at some DLs where MAC1 and MAC2 have also greater values. The most suitable AF can be extracted when all the three MACs have extremely large values. Table 2 implies that such an AF should be searched for upper NVMs (especially for NVM >7), considering the first three DLs. Since MAC1 and MAC2 have relatively good values for large NVMs when the first three levels are regarded, the variation of MAC3 should be examined to decide which level and NVM are suitable. In this connection, Fig. 6 is introduced. Although the fourth DL is useless, it is also considered to highlight better the variation of Ea. According to the plots, MAC3 becomes relatively large at the second and third levels when NVM >7. Also, it seems to converge towards approximately 0.97 at the second level, whereas there is an oscillatory behavior about this value at the third level. However, there seems no noticeable difference between the MAC3s of these levels. Then, making a choice between the second and the third levels is required. In this paper, it is asserted that the second DL is better in comparison to the third one when the following reasons are considered: (1) Variation of MAC3 versus NVM at the second level is more stable than that of the third level. Besides, although MAC3 of the third level has slightly greater values at some higher NVMs, MAC1 and MAC2 also decrease slightly (see Table 2). Moreover, at the third level MAC3 has lower values for some NVMs than it has at the second level, which will be clearer later when other graphs for Daubechies wavelets and other mode shapes are dealt with. (2) As previously stated, MACs between AF and numerically obtained undamaged mode are not available in practice, since one generally have no information about the healthy structure. In this case, it is difficult to decide which DL is appropriate in advance. Hence, an indicator warning that MAC3 has its greatest values is required. Therefore, the variation of Ea wrt NVM and DL is considered, as shown in Fig. 7. Compared to the second level, it is obvious from these plots and Table 2 that the first noticeable drop in Ea occurs at the third level. In this paper, it is proposed that the level before, i.e. the second level, is suitable to obtain an AF which is well estimation of the undamaged mode. Because, MAC3 has sufficiently large values at the second level for higher NVMs, as illustrated in Fig. 6.

On the other hand, when Daubechies wavelets are considered instead of symlets, similar variations for MAC1 and MAC2 are observed for the same mode shape. Thus, for the sake of brevity just the results related

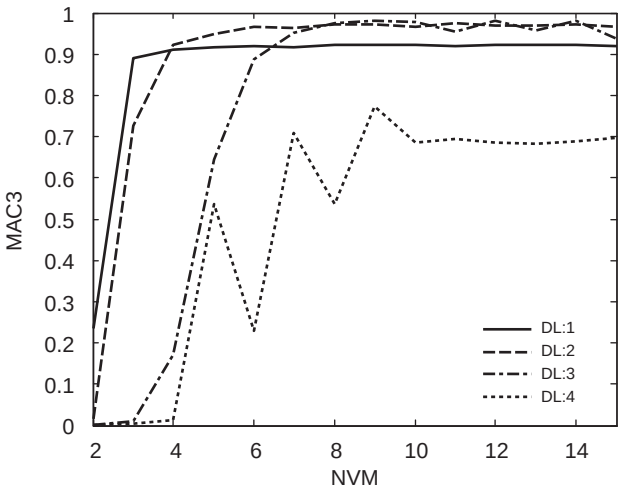

Fig. 6. Variation of MAC3 wrt NVM and DL. Wavelet: symlet, mode: the first numerically obtained damaged mode of the beam in Fig. 5.

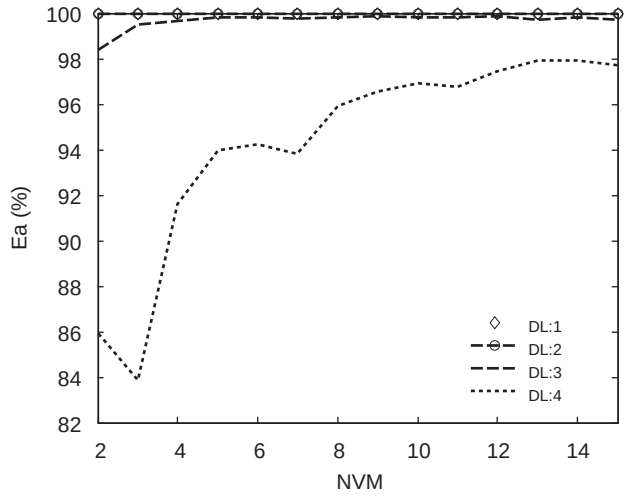

Fig. 7. Variation of Ea wrt NVM and DL. Wavelet: symlet, mode: the first numerically obtained damaged mode of the beam in Fig. 5.

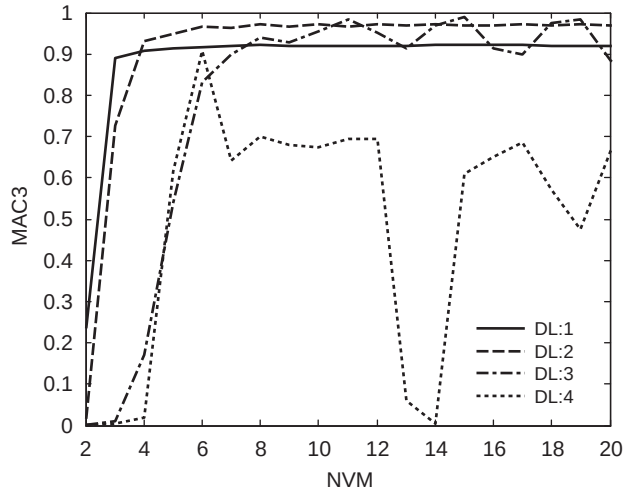

Fig. 8. Variation of MAC3 wrt NVM and DL. Wavelet: Daubechies, mode: the first numerically obtained damaged mode of the beam in Fig. 5.

to MAC3 and Ea are demonstrated in Figs. 8 and 9. The plots, as expected, present similar behavior. Again, the second DL comes out to be suitable for the proper AF, since the first significant drop in Ea occurs at the third level, and MAC3 has comparatively large values for upper NVMs at the second level. In addition, MAC1 and MAC2 are also very large (nearly 0.999) at that level. Although MAC3 at the third level takes greater values for NVM = 11, 15, 19, where MAC1 and MAC2 are nearly 0.99 at the same level, the differences between the MACs of the second and the third levels are of negligible. Besides, as previously stated, MAC3 is both sufficiently high and stable at the level after which the first significant drop in Ea occurs, i.e. the second level, thus this level is at the focus of interest in this work.

Similar procedure is conducted for the second numerically obtained damaged mode of the beam in Fig. 5, considering symlet and Daubechies wavelets, so that similar variations for all MACs and Ea are obtained. Thus, only the Figs. 10–13 are introduced to elucidate the relation between MAC3 and the DL after which the first sharp decrease in Ea occurs. The unsuitability of the third DL is now more apparent as seen in Figs. 10 and 12 (cf. Figs. 6 and 8), since MAC3 is considerably less at the third level for many NVMs.

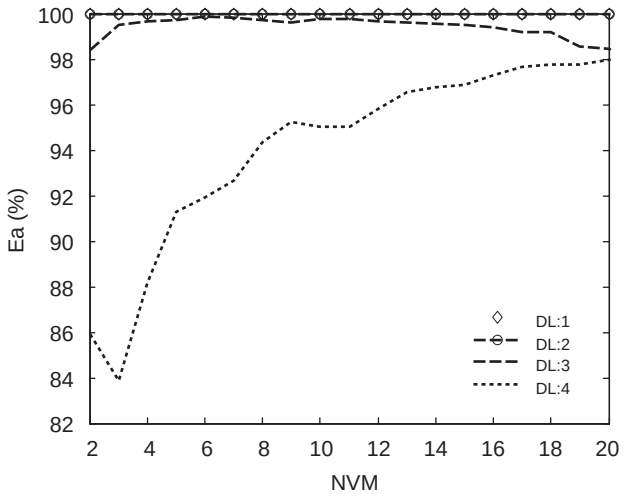

Fig. 9. Variation of Ea wrt NVM and DL. Wavelet: Daubechies, mode: the first numerically obtained damaged mode of the beam in Fig. 5.

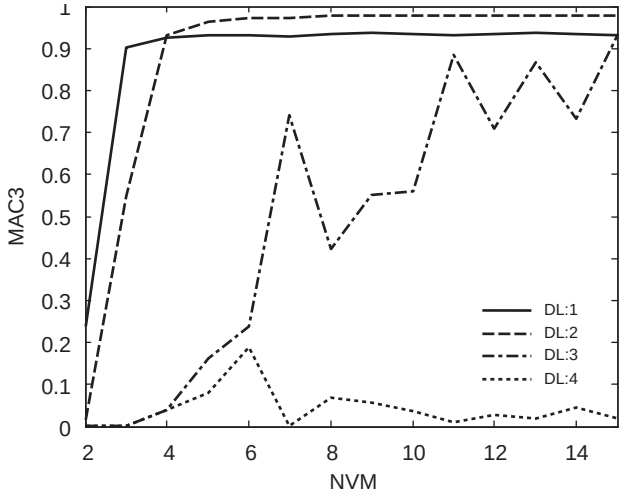

Fig. 10. Variation of MAC3 wrt NVM and DL. Wavelet: symlet, mode: the second numerically obtained damaged mode of the beam in Fig. 5.

When the first two experimental modes of the damaged beam in Fig. 2 are employed, comparable results have come out, as expected. To illustrate the behaviors of MAC3 and Ea, Figs. 14–17 are introduced. For the sake of brevity, only the plots which are obtained by symlet wavelets are demonstrated, since similar results are experienced with Daubechies wavelets. The figures again verify the previously proposed assertion that the DL after which the first notable drop in Ea occurs is the most suitable one, since MAC3 as well as the other MACs become comparatively large at this level, i.e. the second level. However, MAC3 at the second level is now lower compared to the previous graphs for the numerically obtained modes of the beam in Fig. 5. The major reason is certainly the measurement errors, since the experimental method in this work, i.e. the impact testing, is known to be the simplest but the least accurate modal testing approach. Moreover, the number of damages on the beam in Fig. 2 is eight, whereas there are four notches on the beam in Fig. 5, so that the deviations of the experimental modes from the undamaged modes are relatively much. Hence, all MACs are supposed to be lower when the experimental modes are used. On the other hand, the unsuitability of the third level is more apparent, since MAC3 at this level is both relatively lower and unstable.

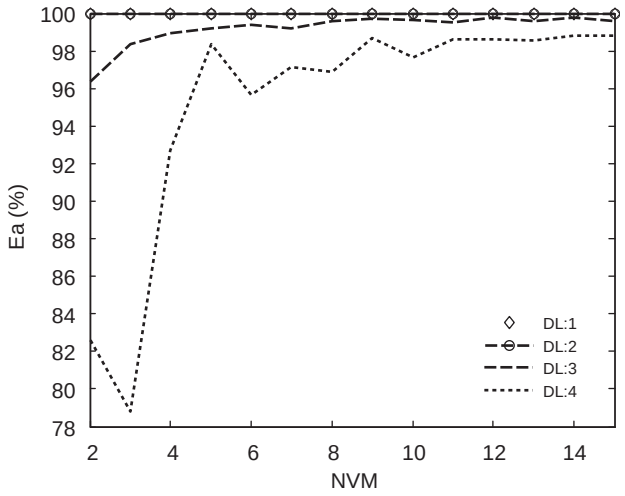

Fig. 11. Variation of Ea wrt NVM and DL. Wavelet: symlet, mode: the second numerically obtained damaged mode of the beam in Fig. 5.

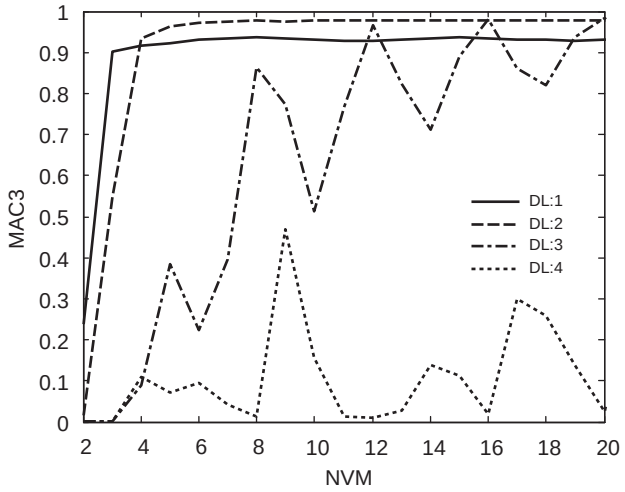

Fig. 12. Variation of MAC3 wrt NVM and DL. Wavelet: Daubechies, mode: the second numerically obtained damaged mode of the beam in Fig. 5.

4.2. Damage detection through the indexes D_1 and D_2

The previous analyses for the four mode shapes revealed that a suitable AF to be used as undamaged beam mode can be extracted, if a symlet wavelet with NVM between the interval 10 and 20 is employed. It was also observed that the second DL should be regarded, since the first notable decrease in Ea appeared at the following level. To figure out how much an AF extracted in this way is suitable, the graphical representations of the damage indexes defined in Eqs. (7) and (8), D_1 and D_2, are illustrated employing these four mode shapes. For that purpose, sym15 wavelet is used to extract the necessary AFs. In addition, each signal was oversampled prior to the CWT to the 10 times of its initial length to enhance spatial resolution, and sym4 wavelet is employed to compute the CWT coefficients.

Firstly, the fundamental numerically obtained damaged mode of the beam in Fig. 5 is considered, and the comparison of the mode shapes with the AF is illustrated in Fig. 18. The MACs and Ea at the second DL for the AF shown in Fig. 18 are computed as MAC1 = 0.9999, MAC2 = 0.9995, MAC3 = 0.9676, Ea = 99.9983.

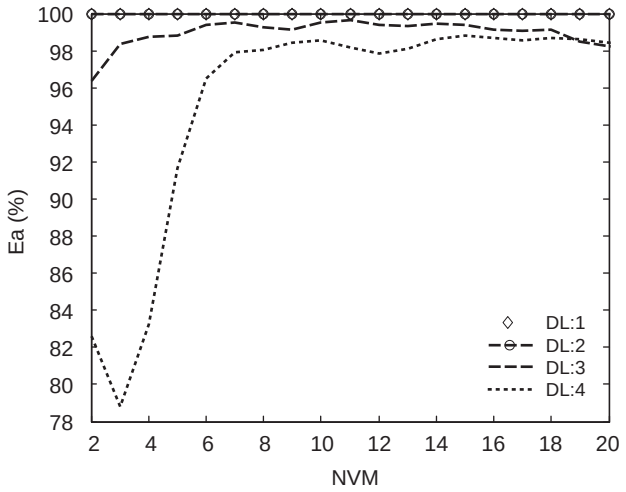

Fig. 13. Variation of Ea wrt NVM and DL. Wavelet: Daubechies, mode: the second numerically obtained damaged mode of the beam in Fig. 5.

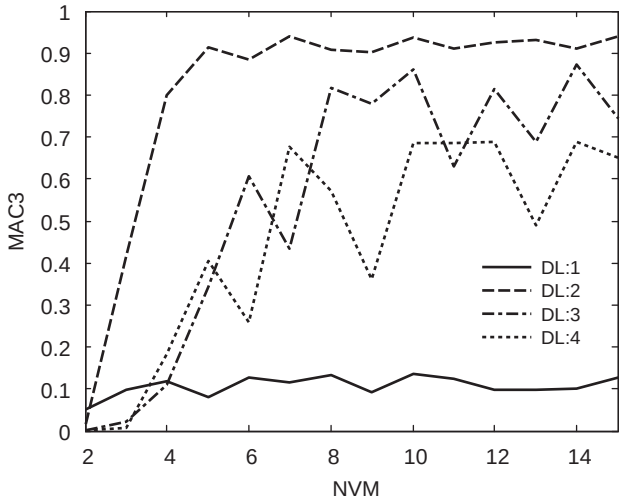

Fig. 14. Variation of MAC3 wrt NVM and DL. Wavelet: symlet, mode: the first experimental mode of the damaged beam in Fig. 2.

From these values and Fig. 18 it is obvious that the extracted AF is in good agreement with the undamaged mode. The normalized variations of the indexes with rising scale are given in Fig. 19 for that mode shape. The number at the top of each graph stands for the scale, while the upright dashed lines denote the damage locations given in the legend of Fig. 5. Although the first notch, which is very close to the left end, is not identified, and there is just a single peak at the proximity of the third and the fourth damage zones as if there is a single damage over there, the agreement of the plots of the indexes are relatively good, which is more apparent in Fig. 20, where the enlarged graph corresponding to the scale 30 is illustrated. On the other hand, the agreement between the indexes seems comparatively good at lower scales, which are more important in damage detection, since damage effect appears generally better localized at lower scales. By the way, the reason of the problem with the first notch is essentially related to the curvature on that location, since magnitude of wavelet coefficient on a damage site is proportional to the curvature on that location.

Secondly, Figs. 21–23 are obtained in a similar fashion, employing the second numerically obtained damaged mode of the beam in Fig. 5. The MACs and Ea for this mode at the second DL were found as

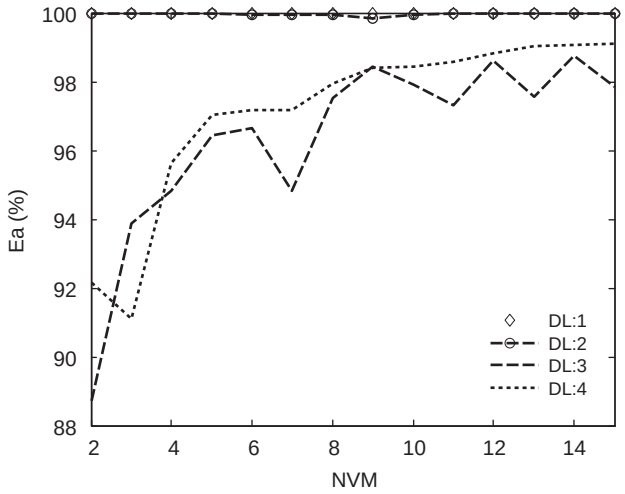

Fig. 15. Variation of Ea wrt NVM and DL. Wavelet: symlet, mode: the first experimental mode of the damaged beam in Fig. 2.

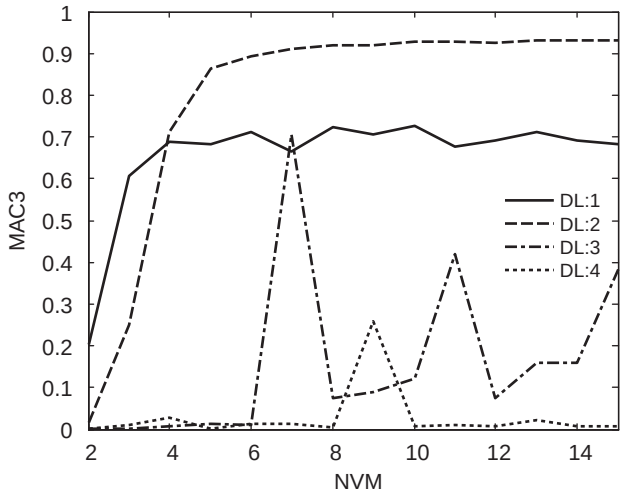

Fig. 16. Variation of MAC3 wrt NVM and DL. Wavelet: symlet, mode: the second experimental mode of the damaged beam in Fig. 2.

MAC1 = 0.9991, MAC2 = 0.9982, MAC3 = 0.9775, Ea = 99.9972. In view of the plots, the first damage is still not detected, while the third and the fourth damage locations are not discriminated. However, the curves corresponding to the indexes are again in well accordance with each other. Although some discrepancies appear at relatively upper scales, the highest peaks occur at the damage locations for both indexes at every scale.

Lastly, the experimental modes of the beam in Fig. 2 are employed, so that Figs. 24–29 are obtained. The comparison of the modes with the AF is shown in Figs. 24 and 27 for the first and the second mode, respectively. The MACs and Ea corresponding to the second DL are MAC1 = 0.9981, MAC2 = 0.9950, MAC3 = 0.9395, Ea(percent) = 99.98 for the first mode, and MAC1 = 0.9963, MAC2 = 0.9927, MAC3 = 0.9304, Ea(percent) = 99.98 for the second mode, respectively. The graphical representations of the indexes D_1 and D_2 are illustrated in Figs. 25 and 28, where upright dashed lines refer to the damage locations given in Table 1. From these figures, it is obvious that D_1 and D_2 are in comparatively good accordance with each other for the first mode. However, the discrepancy between them becomes more pronounced with rising scale for the second mode, as seen in Fig. 28. When the above MACs for these two

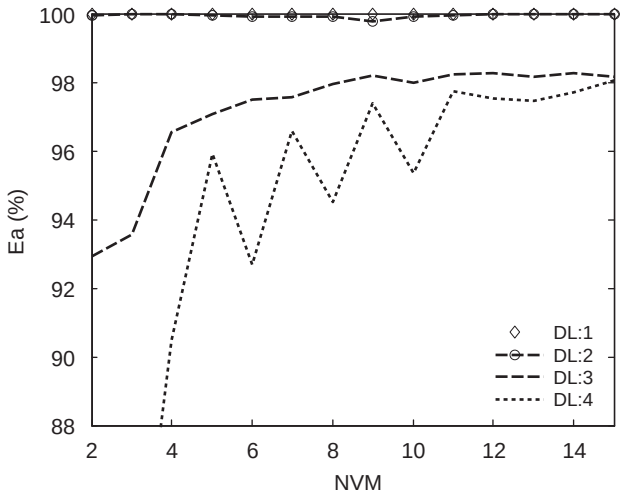

Fig. 17. Variation of Ea wrt NVM and DL. Wavelet: symlet, mode: the second experimental mode of the damaged beam in Fig. 2.

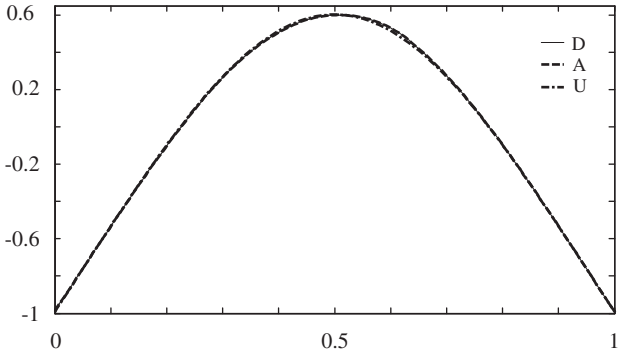

Fig. 18. Comparison of the numerically obtained damaged (D) and the undamaged (U) first modes of the beam in Fig. 5 with the AF (A) extracted from the damaged mode.

modes are compared, the reason of this scene becomes comprehensive, since the MACs for the second mode are lower compared to those of the first mode. On the other hand, it is well-known that damage signature is generally available in small-scale wavelet coefficients, since damage-induced local variations appear as high-frequency components. Thus, the agreement between the two indexes is much more important at the lower scales. When Figs. 25 and 28 are considered, it is clear that this requirement is sufficiently satisfied. Also, Figs. 26 and 29 are introduced for the first and the second mode, respectively, to attract attention to the compatibility of these two indexes.

As to damage detection, the following observations are made: In view of Figs. 25 and 26 only V, VI and VIII are managed to be determined by D_1 and D_2, since the highest peaks are on these locations. Moreover, V and VI can be said to be separately identified, since there are two notable peaks in their neighborhood. On the other hand, Fig. 28 seems to give less information about damage detection, which is mainly due to the more measurement errors and noise. According to Fig. 28, D_2 seems to have captured only the signatures of the damages II, III, IV, V, and VI at upper scales. However, III and IV are not separately identified, rather there seems to be single damage instead, which is also valid for V and VI. On the other hand, only the damage II is properly detected by D_1 at the 50th scale. Nevertheless, if the second mode were more accurately measured, D_1 and D_2 would be as compatible as in Fig. 25.

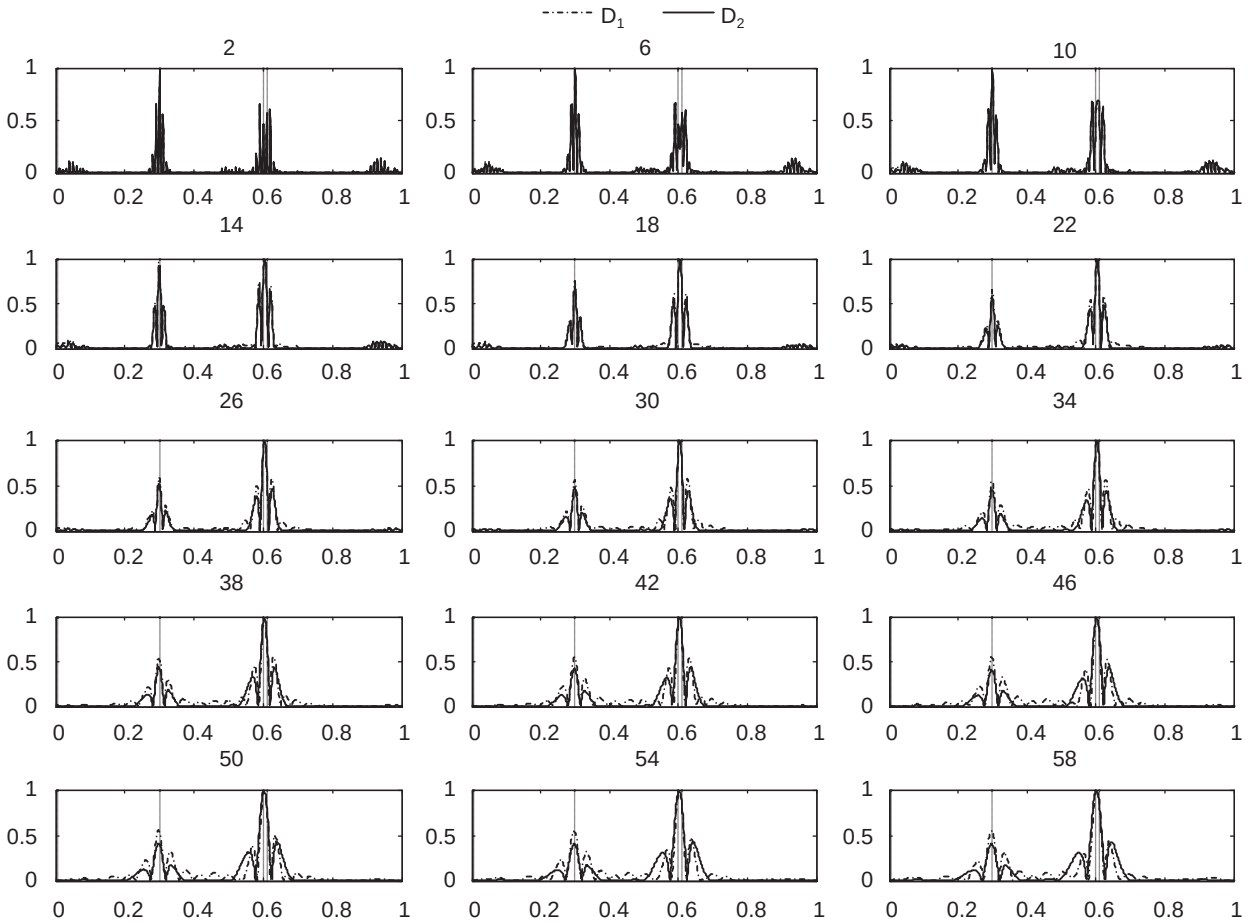

Fig. 19. Damage indexes D_1 and D_2 for the first mode of the beam in Fig. 5.

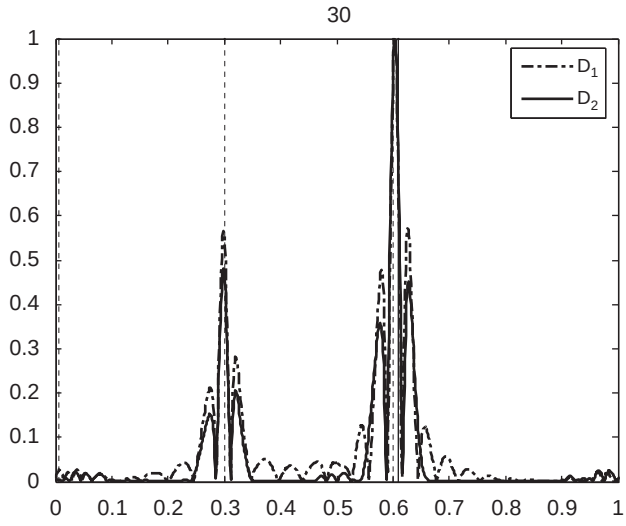

Fig. 20. Damage indexes D_1 and D_2 for the first mode of the beam in Fig. 5 at the 30th scale.

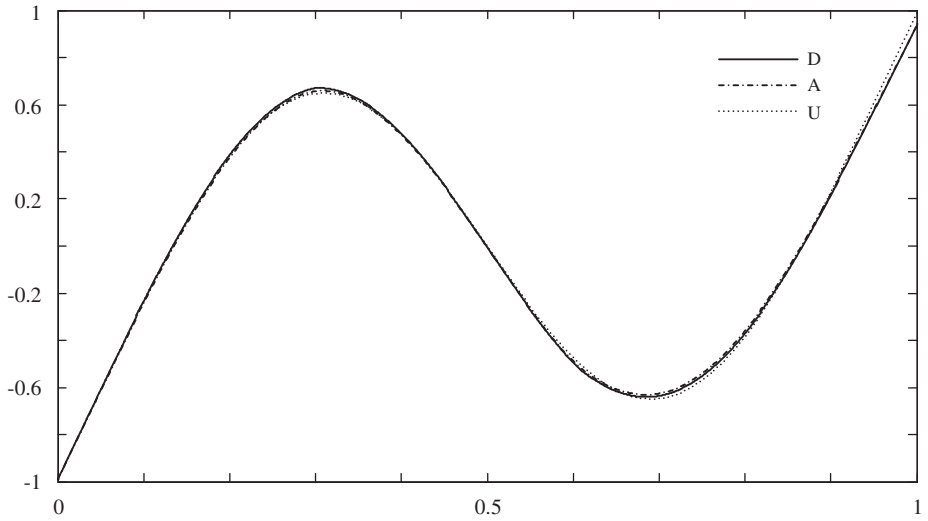

Fig. 21. Comparison of the numerically obtained damaged (D) and the undamaged (U) second modes of the beam in Fig. 5 with the AF (A) extracted from the damaged mode.

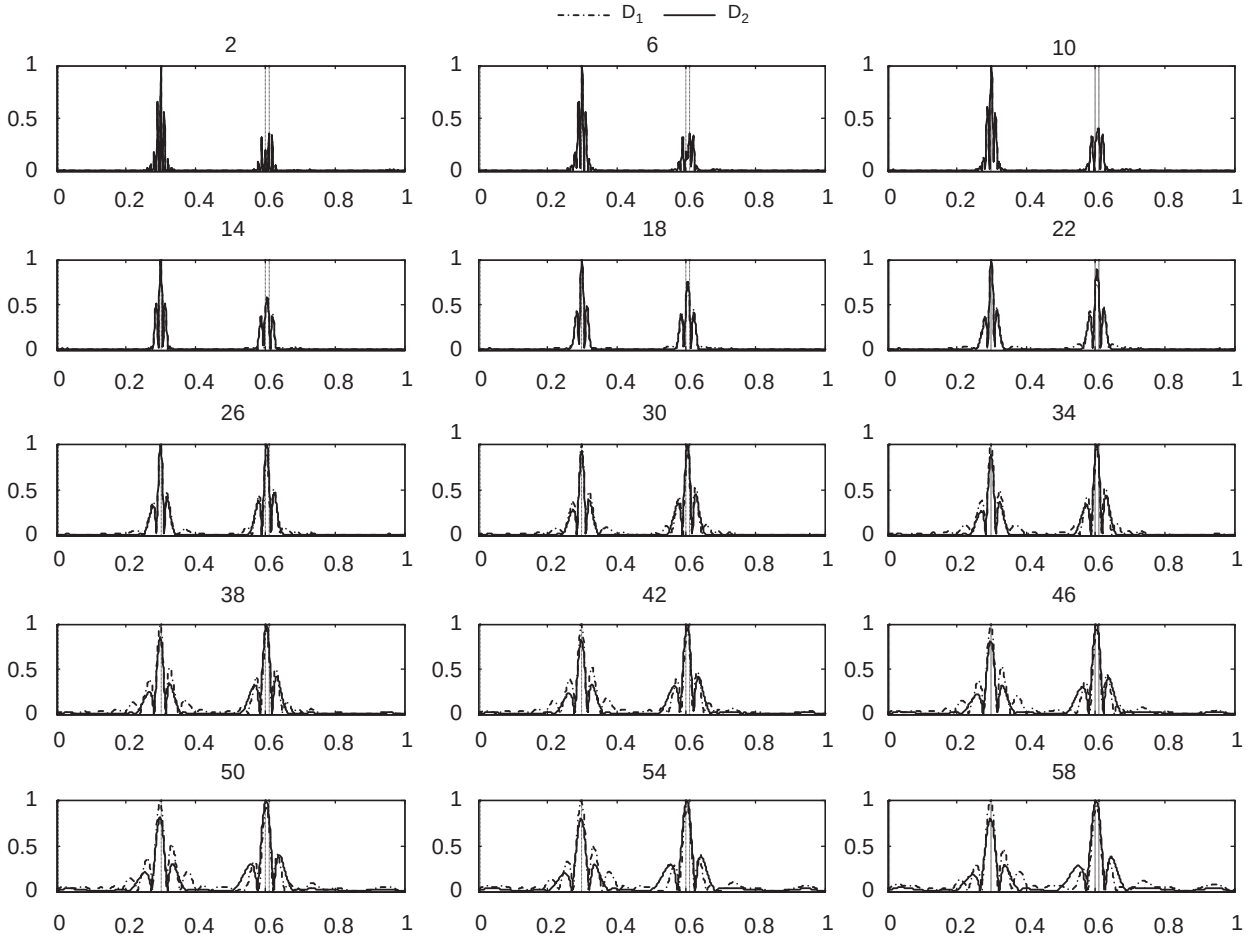

Fig. 22. Damage indexes D_1 and D_2 for the second mode of the beam in Fig. 5.

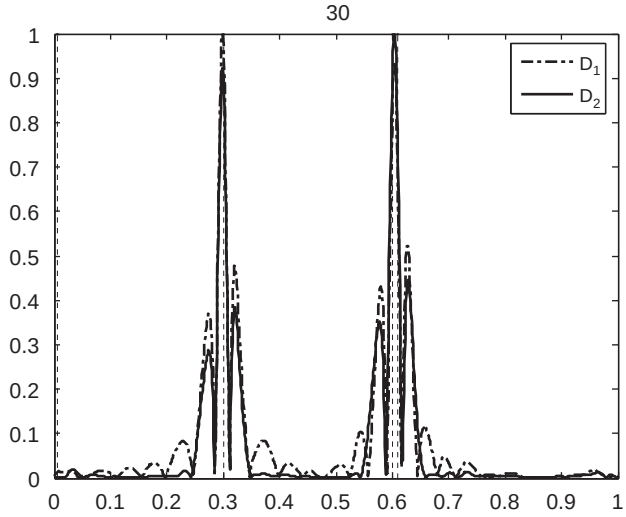

Fig. 23. Damage indexes D_1 and D_2 for the second mode of the beam in Fig. 5 at the 30th scale.

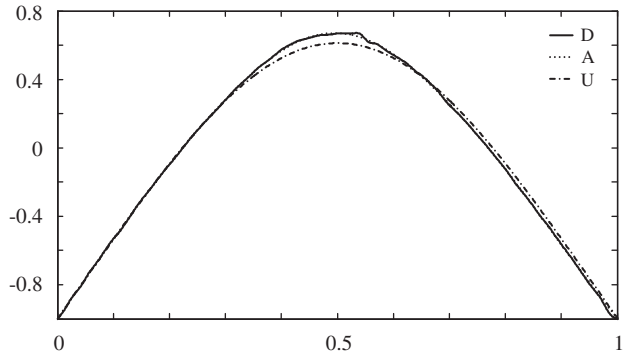

Fig. 24. Comparison of the experimental damaged first mode (D), numerical undamaged first mode obtained by ANSYS (U), and the AF (A) extracted from the damaged mode.

5. Conclusions

In this study, a new wavelet-based damage detection approach for beam-type structures is introduced. According to the method, an approximately equivalent of healthy mode shape can be recovered from damaged one by the DWT, provided a suitable wavelet and a DL are determined. The suitability of an extracted AF is evaluated by means of three MACs defined for the AF, numerical undamaged mode, and their derivatives. Then, a relation between the relatively great values of these MACs and the first notable drop in approximation energy ratio, Ea, is realized; i.e., it was observed that all three MACs have comparatively large values at the decomposition level after which the first significant decrease in Ea comes out, which implies that the AF extracted at this level is a good candidate to be employed as undamaged mode. Some results drawn from the simulations are as follows:

1. A symlet wavelet with a NVM such that $10 < \text{NVM} < 20$, especially the "sym15", is a proper tool to derive the most suitable approximation function by the DWT.

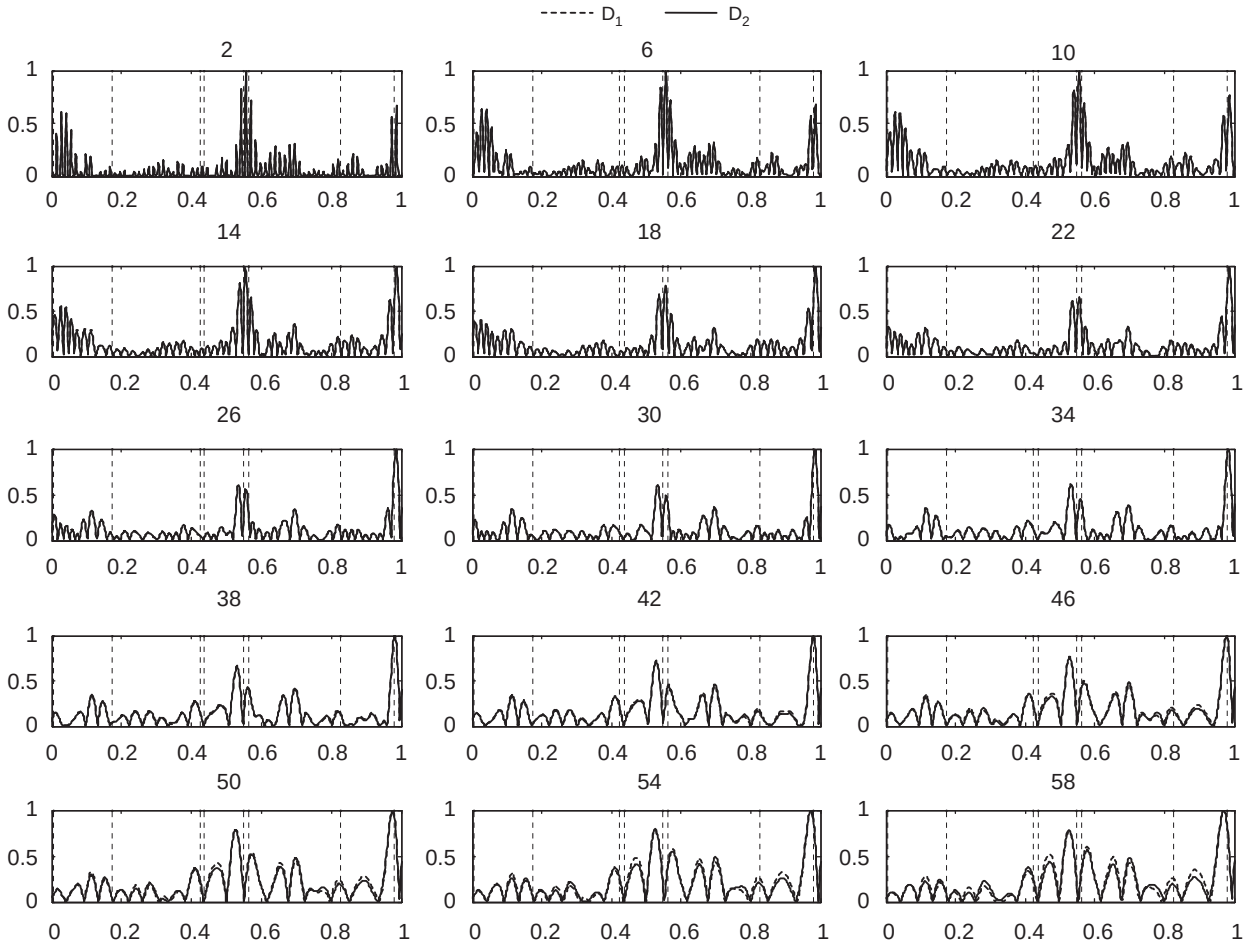

Fig. 25. Damage indexes D_1 and D_2 for the first experimental mode of the beam in Fig. 2.

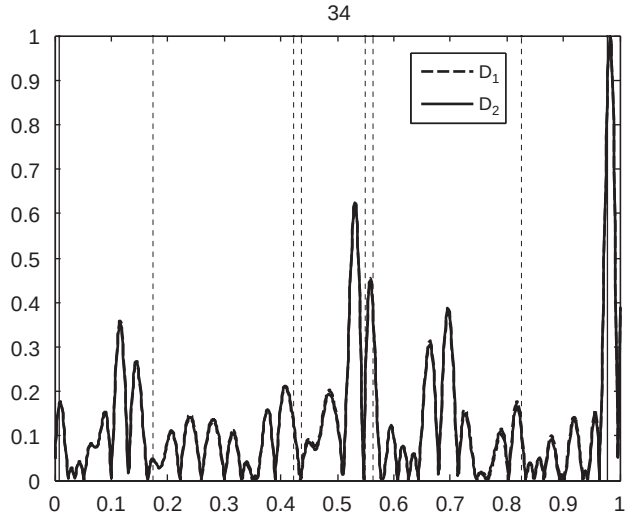

Fig. 26. Variation of D_1 and D_2 for the first experimental mode of the beam in Fig. 2 at the 34th scale.

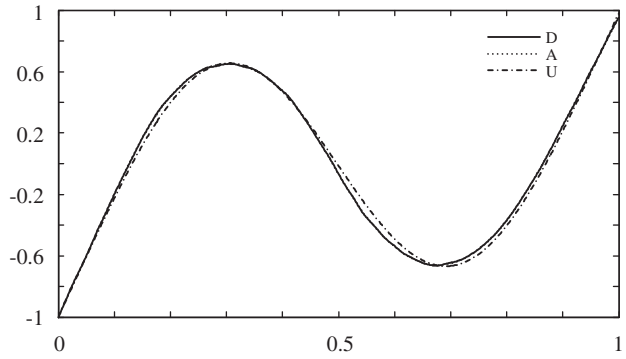

Fig. 27. Comparison of the experimental damaged second mode (D), numerical undamaged second mode obtained by ANSYS (U), and the AF (A) extracted from the damaged mode.

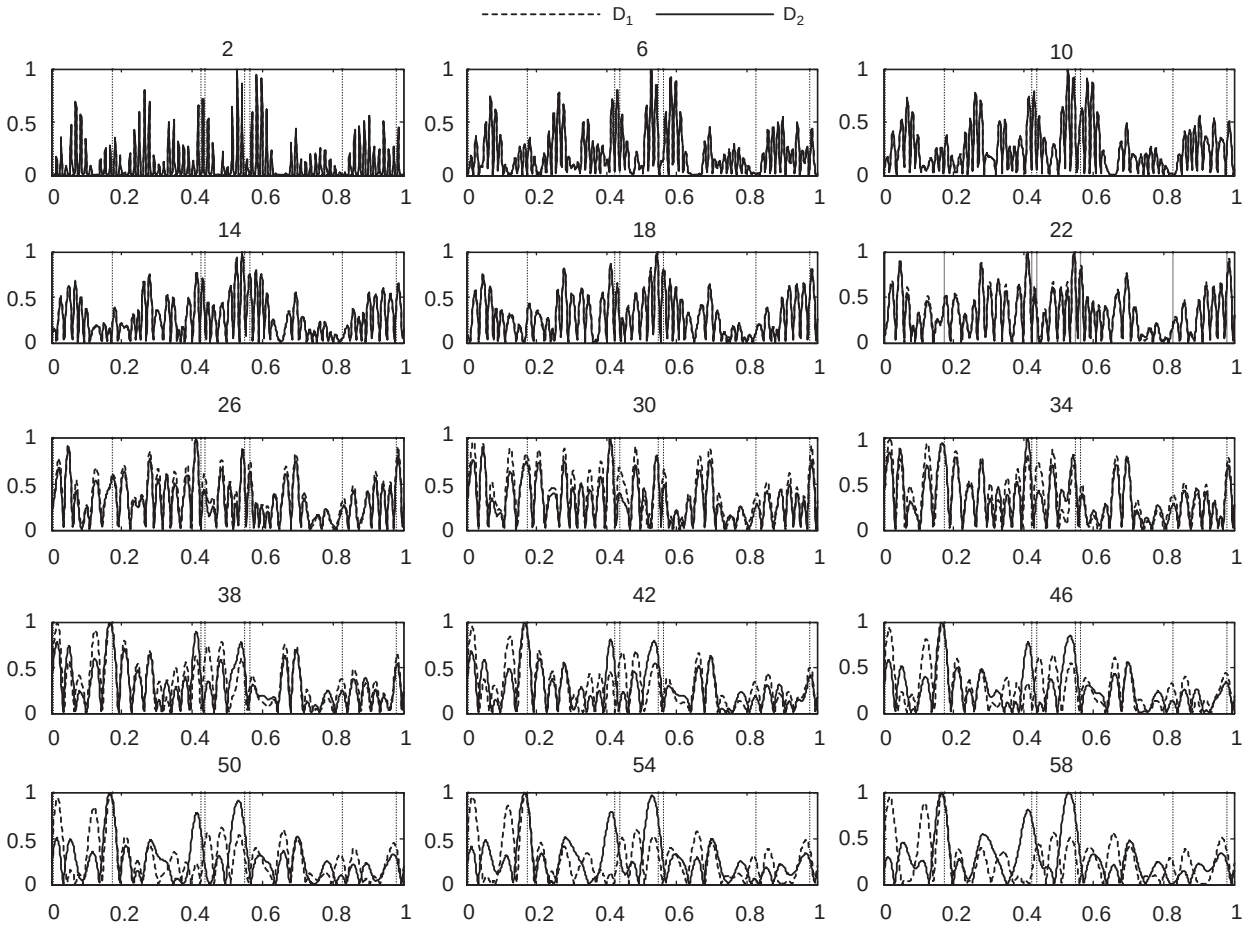

Fig. 28. Damage indexes D_1 and D_2 for the second experimental mode of the beam in Fig. 2.

2. The first notable decrease in Ea was recorded at the third decomposition level for all the four mode shapes, i.e. the second level turned out to be the most suitable, although the lengths of the experimental damaged modes of the beam in Fig. 2 and the numerically obtained damaged modes of the beam in Fig. 5 were different.

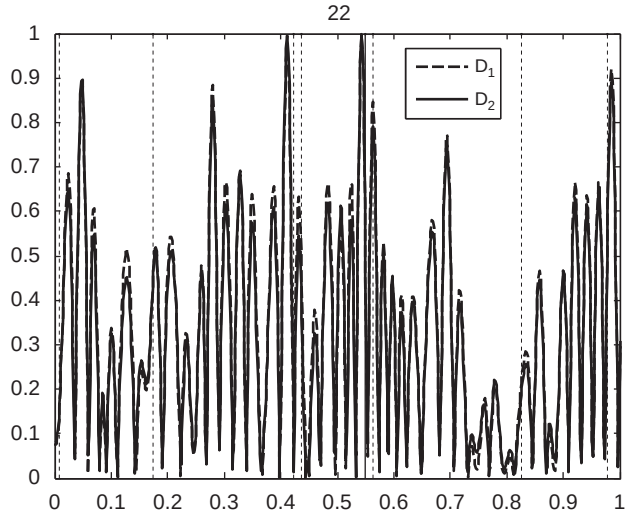

Fig. 29. Variation of D_1 and D_2 for the second experimental mode of the beam in Fig. 2 at the 22nd scale.

3. The more damage extent increases, the less correlation between the damaged and undamaged modes is expected. Thus, the correlation between the extracted AF and undamaged mode decreases with rising damage extent. When the notch number and depths are considered, it can be concluded that the damage extents in this work are of significant order. However, the extracted approximations seem to be relatively compatible with numerical undamaged modes. Therefore, the proposed method is supposed to yield better results for small-size defects or early damages.

The significant drawback of the methods requiring baseline data is that healthy data may not be available in general. Although the proposed method also employs a baseline data, it produces that artificially from damaged one. Thus, it can be deemed as a member of the group of methods employing only the damaged data. On the other hand, the performance of the method should further be assessed by considering other boundary conditions. Moreover, applicability of the method to plate-like bidimensional structures seems worthy of investigation. These issues are planned to deal with in later works.

Acknowledgment

This research was supported by TÜBİTAK under the project 107M371.

References

[1] H. Kim, H. Melhem, Damage detection of structures by wavelet analysis, *Engineering Structures* 26 (2004) 347–362.
[2] Q. Wang, X. Deng, Damage detection with spatial wavelets, *International Journal of Solids and Structures* 36 (1999) 3443–3468.
[3] J.-C. Hong, Y.Y. Kim, H.C. Lee, Y.W. Lee, Damage detection using the Lipschitz exponent estimated by the wavelet transform: applications to vibration modes of a beam, *International Journal of Solids and Structures* 39 (2002) 1803–1816.
[4] E. Douka, S. Loutridis, A. Trochidis, Crack identification in beams using wavelet analysis, *International Journal of Solids and Structures* 40 (2003) 3557–3569.
[5] A. Gentile, A. Messina, On the continuous wavelet transforms applied to discrete vibrational data for detecting open cracks in damaged beams, *International Journal of Solids and Structures* 40 (2003) 295–315.
[6] C.-C. Chang, L.-W. Chen, Vibration damage detection of a Timoshenko beam by spatial wavelet based approach, *Applied Acoustics* 64 (2003) 1217–1240.
[7] A.V. Ovanesova, L.E. Suárez, Applications of wavelet transforms to damage detection in frame structures, *Engineering Structures* 26 (2004) 39–49.
[8] C.-C. Chang, L.-W. Chen, Damage detection of a cracked thick rotating blades by a spatial wavelet based approach, *Applied Acoustics* 65 (2004) 1095–1111.

[9] C.-C. Chang, L.-W. Chen, Damage detection of a rectangular plate by spatial wavelet based approach, *Applied Acoustics* 65 (2004) 819–832.
[10] S. Loutridis, E. Douka, A. Trochidis, Crack identification in double-cracked beams using wavelet analysis, *Journal of Sound and Vibration* 277 (2004) 1025–1039.
[11] C.-C. Chang, L.-W. Chen, Detection of the location and size of cracks in the multiple cracked beam by spatial wavelet based approach, *Mechanical Systems and Signal Processing* 19 (2005) 139–155.
[12] M. Rucka, K. Wilde, Application of continuous wavelet transform in vibration based damage detection method for beams and plates, *Journal of Sound and Vibration* 297 (2006) 536–550.
[13] S. Zhong, S.O. Oyadiji, Crack detection in simply supported beams without baseline modal parameters by stationary wavelet transform, *Mechanical Systems and Signal Processing* 21 (2007) 1853–1884.
[14] E. Castro, M.T. Garcia-Hernández, A. Gallego, Damage detection in rods by means of the wavelet analysis of vibrations: influence of the mode order, *Journal of Sound and Vibration* 296 (2006) 1028–1038.
[15] E. Castro, M.T. Garcia-Hernández, A. Gallego, Defect identification in rods subject to forced vibrations using the spatial wavelet transform, *Applied Acoustics* 68 (2007) 699–715.
[16] X.Q. Zhu, S.S. Law, Wavelet-based crack identification of brige beam from operational deflection time history, *International Journal of Solids and Structures* 43 (2006) 2299–2317.
[17] P.S. Addison, *The Illustrated Wavelet Transform Handbook: Introductory Theory and Applications in Science, Engineering, Medicine and Finance*, IOP Publishing Ltd, London, 2002.
[18] H.-G. Stark, *Wavelets and Signal Processing: An Application-based Introduction*, Springer, The Netherlands, 2005.
[19] A. Messina, Refinements of damage detection methods based on wavelet analysis of dynamical shapes, *International Journal of Solids and Structures* 45 (2008) 4068–4097.
[20] M. Misiti, Y. Misiti, G. Oppenheim, J.-M. Poggi, *Wavelet Toolbox 4 User's Guide*, The Mathworks, Inc.
[21] D.J. Ewins, *Modal Testing: Theory, Practice and Applications*, Research Studies Press Ltd, Baldock, 2000.
[22] L. Debnath, *Wavelet Transforms and Their Applications*, Birkhäuser, Boston, 2002.